MATERIALS CHEMISTRY
FRONTIERS

RESEARCH ARTICLE

Check for updates

Cite this: *Mater. Chem. Front.*, 2019, **3**, 1538

Layer-by-layer growth in solution deposition of monocrystalline lead sulfide thin films on GaAs(111)†

Tzvi Templeman,[a] Maayan Perez,[a] Ofir Friedman,[a] Ran Eitan Abutbul,[a] Michael Shandalov,[b] Vladimir Ezersky,[a] Oleg Konovalov[c] and Yuval Golan*[a]

Received 15th March 2019,
Accepted 17th May 2019

DOI: 10.1039/c9qm00155g

rsc.li/frontiers-materials

We report layer-by-layer growth of single crystal PbS films with unprecedented quality using chemical solution deposition, on par with much more sophisticated growth techniques. *Ex situ* transmission electron microscopy and in-house X-ray diffraction established the monocrystalline nature of the films and the atomically smooth film surface. High brilliance synchrotron X-rays were employed in grazing incidence geometry for *in situ* monitoring the formation of a gallium sulfide interfacial layer, and for establishing layer-by-layer growth of the subsequent PbS film. Our findings show that by maintaining a large reservoir of free sulfide ions, layer-by-layer growth is maintained by reducing the interfacial surface free energy.

Introduction

Epitaxial thin films play a major role in a wide range of technological applications which require pristine quality materials with minimal interfacial defects. As such, the growth techniques and parameters which lead to such pristine quality film growth are continuously subject to vigorous research activities.[1–3] Common growth methods which are used to achieve ultrahigh material quality are derivatives of physical and chemical deposition such as molecular beam epitaxy (MBE) and atomic layer deposition. Such techniques enable full control over the chemical environment, pressure, temperature and growth rate required for achieving epitaxial growth of high quality monocrystalline films.[1,4,5] These requirements make the realization of the films complex and costly. Alternatively, chemical bath deposition (CBD) of semiconductor thin films is among the simplest and least expensive techniques. However, simplicity comes at a cost – CBD is often limited to reagents of lower purity (compared to gas phase precursors) and low temperatures (due to solvent boiling point), and at times results in low purity materials with high defect densities.[6–11]

In CBD of semiconductor thin films, cationic and anionic precursors are dissolved in a solution (commonly aqueous) to react upon a solid substrate. One of the most common growth mechanisms in CBD is 'ion-by-ion' (IBI), where the reaction occurs directly on the substrate *via* heterogeneous nucleation, resulting in films with relatively large grain size. Chemical epitaxy is a term describing growth of thin films from solution with well-defined orientation relations between film and substrate.[12] While monocrystalline semiconductor films with low defect densities grown using simple and inexpensive techniques are highly desired for potential applications, there are a limited number of reports on chemical epitaxy of high quality monocrystalline thin films. Among these reports the lead chalcogenide films were distinguished as having exceptional monocrystalline morphology and grown on a variety of substrates, such as PbS films on Ge, InP, CdS and GaAs single crystal substrates.[12–16] All of these reports have a common motive, where films are obtained *via* IBI growth mode in which 3D islands nucleate and coalesce (Volmer–Weber growth, VW).[6,7,12,17,18] While this process may result in monocrystalline thin films with low surface roughness,[12,18,19] the 3D growth results in internal domains due to low angle misorientations during coalescence of adjacent islands. These internal domains along with high densities of growth induced linear and planar defects all have a critical impact on material physical properties.[2,12,14,18,20] Acquiring high quality epitaxial thin films usually requires layer-by-layer growth mode (Frank van der Merwe, FM), where surface coverage is achieved prior to initiation of a new monolayer. To date, no report exists on epitaxial films grown in FM mode in CBD.

[a] *Department of Materials Engineering and the Ilse Katz Institute of Nanoscale Science and Technology, Ben Gurion University of the Negev, Be'er-Sheva 84105, Israel. E-mail: ygolan@bgu.ac.il*
[b] *Department of Physics, Nuclear Research Center Negev, P.O. Box 9001, Be'er Sheva, Israel*
[c] *Beamline ID10, European Synchrotron Radiation Facility, Grenoble, France*

† Electronic supplementary information (ESI) available. See DOI: 10.1039/c9qm00155g

A unique opportunity arises with the use of high brilliance synchrotron X-ray beams for providing structural information from minute amounts of materials, such as in ultrathin films. Moreover, the high energy X-ray beam can penetrate through liquid media, allowing for *in situ* monitoring of film growth from the very early stages.[21,22] Using a custom designed liquid cell, we have employed high brilliance synchrotron X-rays in grazing incidence geometry for monitoring substrate pre-treatment and subsequent PbS film growth in real time. Grazing incidence X-ray diffraction (GIXD) 'snapshots' were taken during the very early stages of film formation, and further to monitor the structural evolution of the film. Here we present for the first time FM growth of epitaxial PbS films grown from solution on GaAs(111) using CBD.

Results and discussion

PbS thin films were grown on GaAs(111)A (Ga terminated) substrates using CBD and characterized with high resolution scanning electron microscopy (HRSEM, Fig. 1a). Plan view images presented a flat and completely featureless film surface. X-ray diffraction (XRD) showed only peaks corresponding to the first and second order (111) Bragg reflection of PbS (Fig. 1b), and rocking curve peak broadening at full width at half maximum (FWHM, Fig. 1c) presented exceptionally low values, on par with reports on monocrystalline PbS films grown using much more sophisticated techniques, as presented in Table 1.

Examination of film microstructure and film–substrate orientation relations was performed in cross-section using transmission electron microscopy (TEM, Fig. 2). Bend contours originating in the substrate and propagating throughout the film were frequently observed (not presented), a further indication of film quality as grain boundaries and dislocations would interrupt contour propagation.[23] Additionally, both the bright field (BF, Fig. 2a) and HRTEM (Fig. 2b) micrographs presented an atomically flat upper film surface, in agreement with the featureless HRSEM plan-view micrographs. Investigation of the film–substrate interface using both HRTEM (Fig. 2c) and high angle annular dark field (HAADF) scanning TEM (STEM, Fig. 2d) techniques revealed a sharp interface, which was further confirmed by monitoring the composition of the substrate surface pre- and post-initial deposition sequence (Fig. 2e and f), which established complete removal of substrate native oxide. Twinning relations between the film and the substrate are evident when examining the film–substrate interface (Fig. 2c and d). Selected area electron diffraction (SAED) (Fig. 2g and h) verified hetero-twinning relations between film and substrate. Such relations have been reported for PbS/ZnTe[24] and were described in detail by Osherov *et al.* in the PbS/GaAs system,[14] where domain formation and film surface roughening clearly pointed out VW growth which resulted in highly defective films and broad (>1500 arcsec) rocking curves.

An interrupted growth series analyzed *ex situ* using conventional atomic force microscopy (AFM, Fig. S1, ESI†) carried out in air showed that the root mean square (RMS) surface roughness of samples before and after reaction initiation was *circa* 0.6 nm which remained constant throughout film growth. This is consistent with AFM imaging in air showing adsorbed molecules (hydrocarbons, *etc.*) on an otherwise featureless

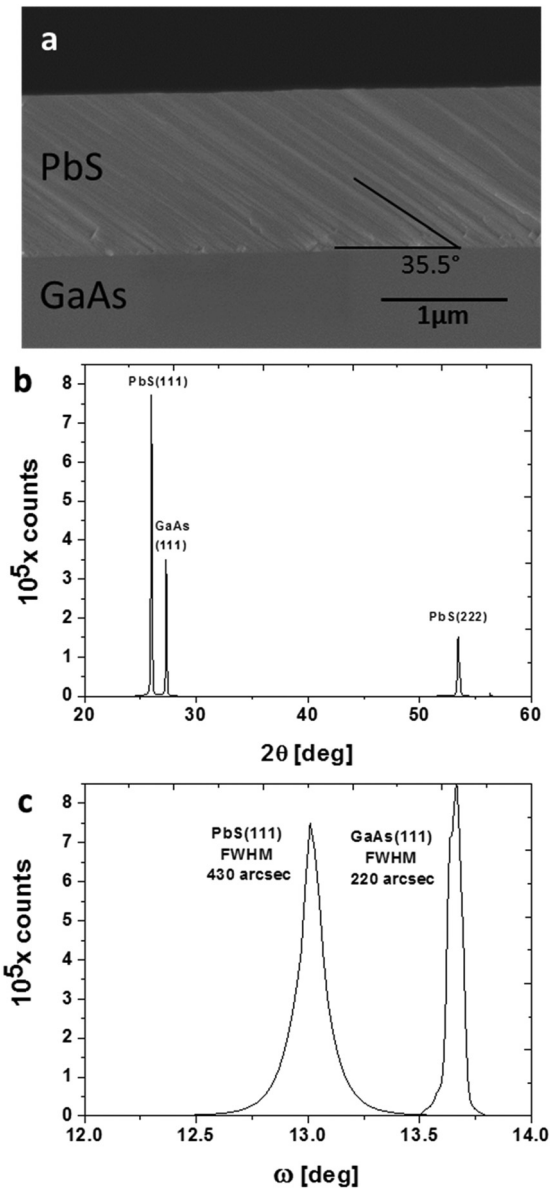

Fig. 1 PbS thin film grown on GaAs(111)A for 2 h. (a) SEM cross section (X-sec) of the cleaved surface showed a 1.3 μm thick film with an array of parallel translation glide planes, indicating high material quality since high densities of structural defects such as domain boundaries would limit glide propagation upon cleavage. Analyzing the crystallographic glide planes is straightforward, considering the (b) single film orientation observed using in-house XRD analysis in $2\theta-\theta$ geometry. The angle of 35.5° between the slip planes and the (111) planes parallel to the film surface identifies them as {110} slip planes, which are common for most NaCl systems.[41] The out-of-plane coherence length, based on Scherrer broadening of the PbS peaks shown in (b), was on par with the instrumental broadening (*circa* 340 arcsec). (c) XRD rocking curve analysis was performed to gain insight into film crystal quality since FM growth is expected to show a low degree of mosaicity and defect density. See Table 1 for comparison with literature values.

Table 1 Comparison of out of plane XRD rocking curve values for single crystal PbS films grown on different substrates using a variety of vapor phase techniques

Growth technique	Substrate	Reflection analyzed	FWHM [arcsec]	Ref.
CBD	GaAs(111)A	(111)	400	Current work
HWE	BaF_2(111)	(111)	200	Zogg[25]
PVT	EuS(100)	(200)	200	Chernyshova[26]
PVT	KCl(100)	(200)	300	Chernyshova[26]
PVT	YbS/Si(100)	(200)	200–300	Fedorenko[27]
PVT	KCl(100)	(200)	300	Fedorenko[27]
MBE	PS/Si(111)	(111)	500	Levchenko[28]
Sublimation	—	(200)	300–400	Tomm[29]

surface, and is nearly identical to the roughness observed for the GaAs(111) substrates used in this work.

To monitor the initial stages of film growth, a custom designed liquid cell was constructed (Fig. S2, ESI† and Fig. 3a) which allowed for real time synchrotron GIXD studies of the growing films. After surface pre-treatment, the deposition reaction was initiated by injection of thiourea and the substrate was rotated step-by-step around the sample surface normal, φ axis (Fig. 3b), keeping fixed the grazing angle of incidence and recording GIXD snapshots at each step using a 2D Pilatus 300K Dectris detector. During the initial first minute of reaction no reflections apart from $(20\bar{2})_{GaAs}$ were observed (Fig. 3c). After 3 min of reaction the first observable signal of the $(\bar{2}20)_{PbS}$ in-plane reflection was obtained from the film, which intensified after 7 min of deposition (Fig. 3d and e). The lattice constant plotted as a function of deposition duration (Fig. 3f) reveals in-plane compression strains which gradually relax with film thickness, common for FM grown epitaxial films,[3,30] which is expected considering the small, ~5% lattice mismatch between GaAs and PbS. Moreover, once the reaction is initiated a noteworthy decrease is observed in the *d*-spacing values of the substrate (Fig. 3f), which occurs due to the reaction of sulfide anions which readily react with the Ga terminated {111} surface of the substrate to form an intermediate layer of cubic GaS. This phase was reported to form epitaxially upon exposure of GaAs substrates to single source precursors such as $Ga(SOCNEt_2)_3$ and $[(^tBu)GaS]_4$, a direct result of the small lattice mismatch of under 3% and the similar face-centered based cubic structures.[31,32] The lattice parameter of cubic GaS is 0.55 nm (compared to 0.56 nm for GaAs) and slightly higher when lattice matched with GaAs substrates.[31,32] The current results indicate instantaneous formation of this phase once the substrate surface is exposed to sulfide anions, which explains why the 0.200 nm *d*-spacing of $(20\bar{2})_{GaAs}$ decreases to 0.195 nm, in good agreement with the reported {220} *d*-spacing of cubic GaS.

Variations in film and substrate reflection intensities *vs.* deposition time were used to monitor the time dependent evolution of film thickness (z), which can be derived from the GaAs$(20\bar{2})$ substrate peak intensity attenuation by the growing film according to the X-ray beam travel through material thickness (z) with a $1/e$ attenuation length (τ):

$$I = I_0 \exp(-z/\tau) \quad (1)$$

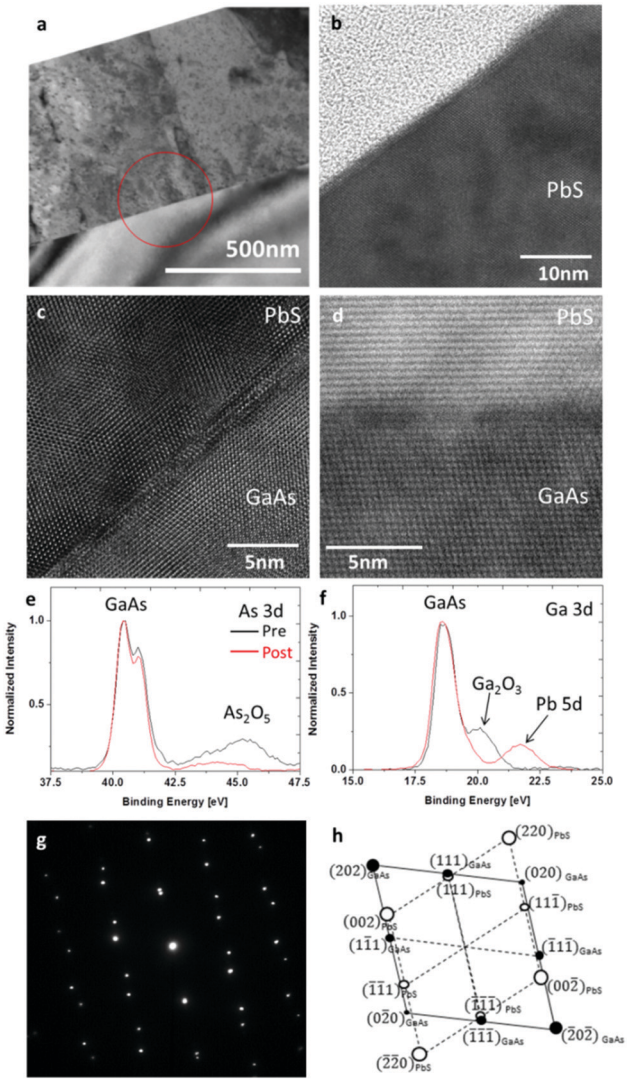

Fig. 2 PbS thin film grown on GaAs(111)A for 1 h. (a) BF TEM presents a defect free monocrystal. (b) HRTEM of the upper film, presenting an atomically flat surface. Twinning relations between the film and the substrate are evident when examining the film–substrate interface using both (c) HRTEM and (d) HAADF STEM imaging. The microscope used is not C_s-corrected, thus delocalization effects prohibit clear interpretation.[23] To overcome this issue lattice imaging using HAADF STEM was performed (d), confirming the sharp interface between film and substrate with no evidence for foreign phases or residual native oxides which were removed prior to reaction during a 10 min treatment of the substrate in alkaline solution. This was confirmed using high resolution X-ray photoelectron spectroscopy (HRXPS) analysis of the GaAs(111)A substrate surface, pre and post 10 min immersion in a solution containing lead nitrate and sodium hydroxide, where monitoring the (e) As 3d and (f) Ga 3d spectra clearly indicates effective removal of native oxides. This step proved to be crucial in subsequent film growth, and has been the subject of several studies.[38,42] Film–substrate orientation relations were established using the SAED (g) pattern taken from the film–substrate interface marked by the red circle in (a). (h) Indexing for the diffraction spots in the $[\bar{1}10]_{PbS}$ and $[\bar{1}01]_{GaAs}$ zone axes, and showing the $(111)_{PbS}\|(111)_{GaAs}$ and $[\bar{1}10]_{PbS}\|[\bar{1}01]_{GaAs}$ orientation relations (GaAs JCPDS#32-0389; PbS JCPDS#05-0592).[43] Consequently, the film/substrate relations may be considered as in twin/matrix relations with a (111) twinning plane (the interface) and a $[\bar{2}11]$ twinning direction.

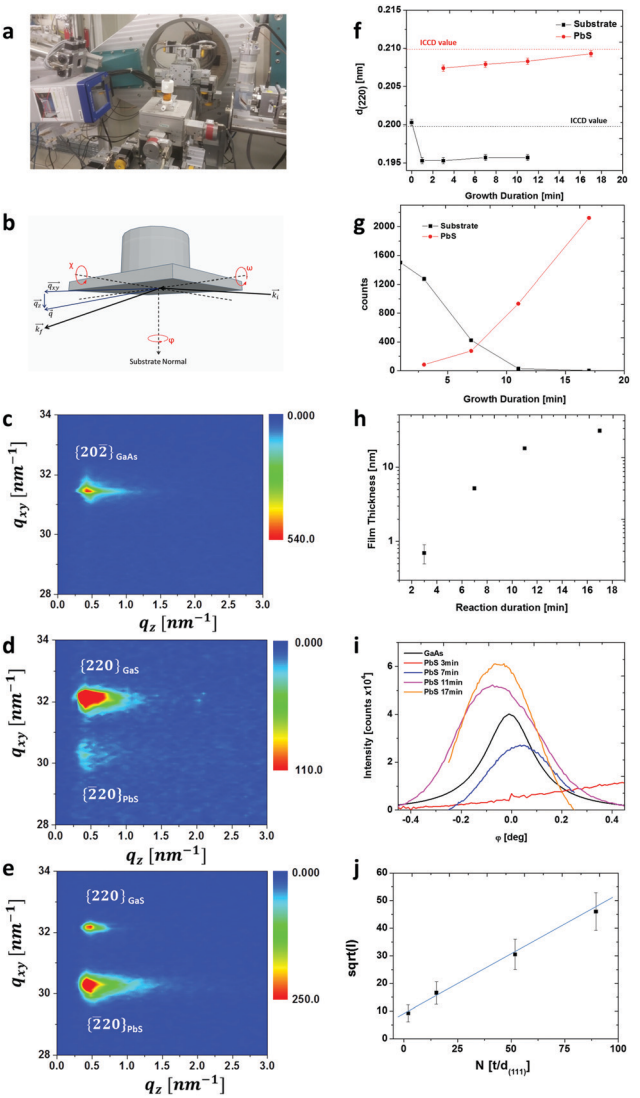

Fig. 3 (a) Photo of the experimental setup at beamline ID10; the cell design is cylindrical with a 0.05 mm Kapton foil serving for both the window and the cell wall (for details see Fig. S2, ESI†). (b) Scattering geometries used in the experiment; the substrate is mounted horizontally facing down, and the cell is fixed on a triple-axis goniometer, allowing control over the X-ray grazing angle, α. The angle α was maintained below the critical angle at 0.08° and the cell was rotated around the normal to the sample surface (φ scans) until the $[\bar{1}\bar{1}2]$ twinning direction was aligned parallel to the incident beam and the GaAs{220} in-plane reflection was recorded along q_{xy}. This point was crucial due to the hetero-twinning nature between film and substrate, which does not allow simultaneous in-plane analysis using the $[10\bar{1}]$ azimuth due to the film–substrate hetero-twinning nature. GIXD snapshots were recorded after (c) 0 min, (d) 3 min and (e) 7 min from reaction initiation. (f) (220) d-spacing of film and substrate as a function of growth duration. (g) $(20\bar{2})_{GaAs}$ and $(\bar{2}20)_{PbS}$ reflection intensities *versus* growth duration. As expected, the intensity from the GaAs substrate is maximal before reaction initiation, and decreases with deposition time. On the other hand, the intensity from the film appears after 3 minutes from initiation and increases with time. (h) Film thickness (attenuation analysis described in the text) as a function of growth duration. (i) $(\bar{2}20)_{PbS}$ intensity as a function of φ rotation angle at increasing growth durations. (j) Square root of the $(\bar{2}20)_{PbS}$ scattering intensity as a function of N_z, the number of repeating units in the z direction, pointing out to layer-by-layer growth mode.

Reflection intensities of $(20\bar{2})_{GaAs}$ were taken prior to reaction initiation as I_0 and during film growth as I.

Below the critical angle (α_c) the incoming electromagnetic radiation propagates along the substrate surface as an evanescent wave, in which the z component of the wave vector is exponentially dampened by the film and the absorption depth can be calculated using the imaginary component of the wave vector.[33]

$$\tau = \frac{\sqrt{2}\lambda}{4\pi}\left[\sqrt{(\alpha^2-\alpha_c{}^2)^2+4\beta^2}-(\alpha^2-\alpha_c{}^2)\right]^{-1/2} \quad (2)$$

where α is the X-ray angle of incidence, λ is the wavelength and β is the imaginary component of the refraction index. Film thicknesses extracted according to eqn (1) are represented as a function of reaction time in Fig. 3h. The imaginary component of the refraction index (β) for PbS was calculated to be 1.946×10^{-7} at 22 keV.[34] Using small angle approximation the critical angle in radians can now be calculated according to

$$\alpha_c \approx \sqrt{2\cdot(\delta_{PbS}-\delta_{H_2O})} \quad (3)$$

with the real component of the refraction index (δ) calculated for 22 keV to be 4.765×10^{-7} and 2.646×10^{-6} for water and PbS, respectively.[34] These values yield a critical angle of $\alpha_c = 0.12°$ for the water/PbS interface, which was used in eqn (2). The resulting film thickness values along with all GIXD *in situ* structural data are presented in Table 2. Note that the film thickness of 0.7 nm extracted for a duration of 3 min of reaction corresponds to the thickness of a PbS bilayer along the ⟨111⟩ axis. The thickness continued to increase to a value of 30.7 nm after 17 min of deposition, which was accompanied by a slight broadening of the rocking curve of the in-plane (220) Bragg reflection. Additionally, the in-plain coherence length (L_{xy}) values are maintained within the range of 100–160 nm. Examining φ in-plane rocking curves performed on the $(\bar{2}20)_{PbS}$ reflection (Fig. 3i) strengthens these results as at ∼3 min of reaction the very first observable signal from the film was recorded. Note that while φ is continuously scanned, film deposition is ongoing. Thus, the continuous increase in $I(\varphi)$ observed for the "PbS 3 min" curve in Fig. 3i corresponds to

Table 2 Structural evolution of the PbS film extracted from *in situ* GIXD measurements. Errors: calculation methods following the theory of errors are described in the ESI. The in-plain coherence length was calculated according to $L_{xy} = 0.9\frac{2\pi}{\mathrm{fwhm}_{q_{xy}}}$, where $\mathrm{fwhm}_{q_{xy}}$ is the full width at half maximum of the Bragg peaks along q_{xy}. Rocking curve error was taken as φ scan resolution

Step	Thickness [nm] ±0.2	$\varphi_{(220)}$ rocking curve [arcsec] ±72	L_{xy} [nm] ±5	$d_{(220)}$ [nm] ±4 × 10^{-4}
GaAs (pre-deposition)	—	828	170	0.2003
PbS (3 min)	0.7	—	105	0.2074
PbS (7 min)	5.2	1656	157	0.2079
PbS (11 min)	17.8	1584	135	0.2083
PbS (17 min)	30.7	1872	118	0.2093

increasing coverage of the substrate, which explains why a peak maximum in $I(\varphi)$ was not observed in the red curve in Fig. 3i.

To verify layer-by-layer growth mode acquired scattering intensities from the film were analyzed as a function of film thickness, considering that the film is a crystal. Scattering intensity from the crystalline film can be described as[35]

$$I = |F|^2 \cdot \frac{\sin^2(\pi N_x h_x)}{\sin^2(\pi h_x)} \cdot \frac{\sin^2(\pi N_y h_y)}{\sin^2(\pi h_y)} \cdot \frac{\sin^2(\pi N_z h_z)}{\sin^2(\pi h_z)} \quad (4)$$

where N is the number of repeating hkl planes, h is a vector describing deviations from Bragg conditions in the x, y and z directions, and F is the structure factor. During layer-by-layer film growth, once initial bilayer coverage is completed, the beam footprint does not change. As such, the contribution to the scattering from in-plane film parameters (N_x,h_x,N_y,h_y) remains constant and can be defined as I_S.

$$I_S \equiv |F|^2 \cdot \frac{\sin^2(\pi N_x h_x)}{\sin^2(\pi h_x)} \cdot \frac{\sin^2(\pi N_y h_y)}{\sin^2(\pi h_y)} \quad (5)$$

The overall intensity I can now be defined as I_S multiplied by the scattering intensity in the z direction

$$I = I_S \cdot \frac{\sin^2(\pi N_z h_z)}{\sin^2(\pi h_z)} \quad (6)$$

At the maximum reflection intensity, *i.e.*, exact Bragg reflection, $h_z = 0$ must take place and therefore

$$I = I_S \cdot \frac{(\pi N_z h_z)^2}{(\pi h_z)^2} = I_S \cdot N_z^2 \quad (7)$$

with layer-by-layer growth in the z direction (out of plane) we can say that N_z, the number of repeating units in the z direction, is

$$N_z = t/d_{(111)} \quad (8)$$

where t is the film thickness and $d_{(111)}$ is the repeating d-spacing. Substituting for N_z gives us the following formula which can be used to validate layer-by-layer growth:

$$\sqrt{I} = \sqrt{I_S} \cdot \frac{t}{d_{(111)}} \quad (9)$$

Representation of film scattering intensities as a function of film thickness is presented in Fig. 3j, clearly pointing to the relation between sqrt(I) and the number of repeating unit cells. Alternatively, in polycrystalline nucleation and growth a linear dependency of I on film thickness is expected (derived in the ESI†). These *in situ* results validate that layer-by-layer growth is maintained throughout film growth. Both the coherence length and rocking curve mosaicity agree with the *ex situ* XRD analysis (Fig. 1), presenting values on par with the high-quality GaAs single crystal substrate. Additionally, low diffuse scattering is observed in the reciprocal space maps for $(\bar{2}20)_{PbS}$ which reaffirms very high film quality.

Earlier studies performed on the PbS/GaAs system presented identical orientation relationships. However as stated above, the growth mode was VW which clearly hampered film quality.[6,7,12,14,17,18] Comparison of the growth conditions presents a prominent difference in [OH^-], which in this work was an order of magnitude higher than previously used, pointing to increased pH as the root cause for this change in growth mode. Hydroxides have two distinct and competing roles in the reaction solution, complexing the cations and thus decreasing the growth rate, and on the other hand reacting with thiourea molecules which releases sulfide ions and thus accelerating the growth rate.[6,8,17]

As a result, the growth rate as a function of pH has a maximum point, where up to a critical pH value the rate increases (anion limited growth); above this value, the rate decreases with pH (cation limited growth). This behavior is not system dependent and has been reported for several material systems such as CdS, CdSe, PbS, and PbSe.[6,17,19,36] In the current system cation limited growth was achieved by increasing the pH, resulting in high concentrations of free sulfide ions. Sulfides, in addition to reacting with lead cations to give PbS, can be used both as surface passivating agents, and as growth assisting surfactants for III–V semiconductors.[44] This is achieved by bonding to surface sites, thus reducing surface energy.[37–40] So far, all our attempts to repeat this growth mode in the PbSe/GaAs system have not been successful, which emphasizes the role of sulfides as surface active growth assisting anions.

Conclusions

Single crystal epitaxial films were grown using chemical deposition upon GaAs(111)A substrates. The growth mechanism was investigated using a combination of both *ex situ* and *in situ* techniques, all of which indicate FM growth mode, unprecedented for CBD. Structural analysis performed on the monocrystalline PbS films obtained indicated very high crystal quality with low defect concentrations, comparable to complex and highly expensive alternative growth techniques. The development of a custom built GIXD cell enabled *in situ* characterization from the earliest stages of growth, for verifying 2D growth and providing key insights regarding developing film mosaicity, coherence length and in-plain strain. The key contributor for FM growth was identified as the high solution pH which induces a large reservoir of free sulfide ions ready to react and passivate substrate and growing film surfaces. Although presented for a specific material system the current growth mechanism is likely to be viable also for other film–substrate pairs, depending on lattice mismatch, polarity and chemical compatibility. High quality single crystals deposited using simple and inexpensive techniques should have a large impact at the fundamental as well as the technological level.

Conflicts of interest

There are no conflicts to declare.

Acknowledgements

Expert assistance from Dr N. Froumin (XPS), Dr D. Mogilyanski (XRD) and Mr J. Jopp (AFM) is gratefully acknowledged. We thank Ben Arush for the design and manufacturing of the GIXD cell. We are grateful to ESRF for providing beamtime at beamline ID10. This work has been supported by the Israel Science Foundation under Grant No. 156/14.

References

1 J. R. Arthur, *Specimen Handling, Preparation, and Treatments in Surface Characterization*, Springer, 1998, pp. 239–293.
2 H. Brune, *Surface and Interface Science: Solid-Solid Interfaces and Thin Films*, Wiley, 2014, pp. 421–491.
3 M. Lorenz, H. Wei, F. Jung, S. Hohenberger, M. Grundmann, C. Patzig, S. Selle and T. Höche, Two-dimensional Frank–van der Merwe growth of functional oxide and nitride thin film superlattices by pulsed laser deposition, *J. Mater. Res.*, 2017, **32**, 3936–3946.
4 J. A. Venables, G. D. T. Spiller and M. Hanbucken, Nucleation and growth of thin films, *Rep. Prog. Phys.*, 1984, **47**, 399–459.
5 J. E. Ayers, *Heteroepitaxy of Semiconductors: Theory, Growth, and Characterization*, CRC Press, Boca Raton, FL, 2nd edn, 2007.
6 G. Hodes, *Chemical Solution Deposition of Semiconductor Films*, Marcel Dekker, INC., NJ, USA, 2002.
7 R. S. Mane and C. D. Lokhande, Chemical deposition method for metal chalcogenide thin films, *Mater. Chem. Phys.*, 2000, **65**, 1–31.
8 D. Lincot, M. Froment and H. Cachet, *Advances in Electrochemical Science and Engineering*, Wiley-VCH Verlag, Weinheim, Germany, 1999, pp. 165–235.
9 M. Froment, H. Cachet, H. Essaaidi, G. Maurin and R. Cortes, Metal chalcogenide semiconductors growth from aqueous solutions, *Pure Appl. Chem.*, 2007, **69**, 77–82.
10 M. Froment and D. Lincot, Phase formation processes in solution at the atomic level: metal chalcogenide semiconductors, *Electrochim. Acta*, 1995, **40**, 1293–1303.
11 M. Froment, Study of CdS Epitaxial Films Chemically Deposited from Aqueous Solutions on InP Single Crystals, *J. Electrochem. Soc.*, 2006, **142**, 2642.
12 A. Osherov and Y. Golan, Chemical epitaxy of semiconductor thin films, *MRS Bull.*, 2010, **35**, 790–796.
13 J. L. Davis and M. K. Norr, Ge-epitaxial-PbS heterojunctions, *J. Appl. Phys.*, 1966, **37**, 1670–1674.
14 A. Osherov, V. Ezersky and Y. Golan, Hetero-Twinning in Chemical Epitaxy of PbS Thin Films on GaAs Substrates, *Cryst. Growth Des.*, 2012, **12**, 4006–4011.
15 M. Isshiki, T. Endo, K. Masumoto and Y. Usui, Epitaxial Growth of PbS Thin Films from Aqueous Solution, *J. Electrochem. Soc.*, 1990, **137**, 2697–2700.
16 S. Watanabe and Y. Mita, CdS–PbS Heterojunctions, *J. Electrochem. Soc.*, 1969, **116**, 989–993.
17 T. Templeman, M. Biton, T. Safrani, M. Shandalov, E. Yahel and Y. Golan, Chemically deposited PbSe thin films: factors deterring reproducibility in the early stages of growth, *CrystEngComm*, 2014, **16**, 10553–10559.
18 A. Osherov, M. Shandalov, V. Ezersky and Y. Golan, Epitaxy and orientation control in chemical solution deposited PbS and PbSe monocrystalline films, *J. Cryst. Growth*, 2007, **304**, 169–178.
19 A. Osherov, V. Ezersky and Y. Golan, The role of solution composition in chemical bath deposition of epitaxial thin films of PbS on GaAs(100), *J. Cryst. Growth*, 2007, **308**, 334–339.
20 C. D. Lokhande, Chemical deposition of metal chalcogenide thin films, *Mater. Chem. Phys.*, 1991, **27**, 1–43.
21 Y. Lifshitz, O. Konovalov, N. Belman, A. Berman and Y. Golan, Template growth of nanocrystalline PbS, CdS, and ZnS on a polydiacetylene langmuir film: an *in situ* grazing incidence X-ray diffraction study, *Adv. Funct. Mater.*, 2006, **16**, 2398–2404.
22 Y. Lifshitz, Y. Golan, O. Konovalov and A. Berman, Structural transitions in polydiacetylene langmuir films, *Langmuir*, 2009, **25**, 4469–4477.
23 D. Williams and C. Carter, *The Transmission Electron Microscope*, Springer, NY, USA, 1996.
24 S. Sengupta, T. Templeman, M. Shandalov, V. Ezersky, C. Chen, E. Moon, J. Phillips and Y. Golan, Chemical epitaxy and interfacial reactivity in solution deposited PbS on ZnTe, *J. Mater. Chem. C*, 2016, **4**, 1996–2002.
25 H. Zogg, C. Maissen, S. Blunier, J. Masek, V. Meyer and R. Pixley, Properties of IV–VI Narrow Gap Semiconductors on Fluoride Covered Silicon, *MRS Proc.*, 1990, **198**, 451–456.
26 M. Chernyshova, E. Lusakowska, V. Domukhovski, K. Grasza, A. Szczerbakow, S. Wrotek, L. Kowalczyk, T. Story, C. J. P. Smits, H. J. M. Swagten, W. J. M. De Jonge, W. Palosz, A. Y. Sipatov and V. V. Volobuev, *Acta Phys. Pol., A*, 2002, **102**, 609–615.
27 A. I. Fedorenko, A. G. Fedorov, A. Y. Sipatov and O. A. Mironov, The epitaxial growth of IV–VI heterostructures and superlattices on (001)Si, *Thin Solid Films*, 1995, **267**, 134–137.
28 V. I. Levchenko, L. I. Postnova, V. P. Bondarenko, N. N. Vorozov, V. A. Yakovtseva and L. N. Dolgyi, Heteroepitaxy of PbS on porous silicon, *Thin Solid Films*, 1999, **348**, 141–144.
29 Y. Tomm, A. Engel and A. M. Gaskov, Structure and Composition of Polished PbS Surfaces, *Cryst. Res. Technol.*, 1986, **21**, 71–78.
30 V. H. Etgens, M. Sauvage-Simkin, R. Pinchaux, J. Massies, N. Jedrecy, A. Waldhauer, S. Tatarenko and P. H. Jouneau, ZnTe/GaAs(001): growth mode and strain evolution during the early stages of molecular-beam-epitaxy heteroepitaxial growth, *Phys. Rev. B: Condens. Matter Mater. Phys.*, 1993, **47**, 10607–10612.
31 A. H. Graeme, M. R. Lazell and P. O'Brien, Deposition of Thin Films of Gallium Sulfide from a Novel Single-Source Precursor, $Ga(SOCNEt_2)_3$, by Aerosol-Assisted CVD, *Chem. Vap. Depos.*, 1999, **5**, 203.
32 A. N. MacInnes, M. B. Power and A. R. Barron, Chemical Vapor Deposition of Gallium Sulfide: Phase Control by Molecular Design, *Chem. Mater.*, 1993, **5**, 1344–1351.
33 M. Birkholz, *Thin Film Analysis by X-ray Scattering*, Wiley-VCH Verlag, Weinheim, Germany, 2006.

34 B. L. Henke, E. M. Gullikson and J. C. Davis, X-ray interactions: photoabsorption, scattering, transmission, and reflection at E = 50–30 000 eV, Z = 1–92, *At. Data Nucl. Data Tables*, 1993, **54**, 181–342.
35 D. K. Bowen and B. K. Tanner, *High resolution X-ray diffractometry and topography*, Taylor & Francis, London, 2005.
36 O. Friedman, D. Korn, V. Ezersky and Y. Golan, Chemical epitaxy of CdSe on GaAs, *CrystEngComm*, 2017, **19**, 5381–5389.
37 O. Takahisa, Passivation of GaAs(001) surfaces by chalcogen atoms (S, Se and Te), *Surf. Sci.*, 1991, **255**, 229–236.
38 D. Zahn, T. Kampen, S. Hohenecker and W. Braun, GaAs surface passivation by ultra-high vacuum deposition of chalcogen atoms, *Vacuum*, 2000, **57**, 139–144.
39 G. W. Anderson, P. Ma and P. R. Norton, The growth of Fe on sulphur passivated Ge(100): a technique for avoiding intermixing, *J. Appl. Phys.*, 1996, **79**, 5641.
40 D. Kandel and E. Kaxiras, in *Solid State Physics – Advances in Research and Applications*, ed. H. Ehrenreich and F. Spaepen, Academic Press, 2000, vol. 54, pp. 219–262.
41 A. Kelly and K. M. Knowles, *Crystallography and Crystal Defects*, Wiley, West Sussex, UK, 2012.
42 M. Rei Vilar, J. El Beghdadi, F. Debontridder, R. Artzi, R. Naaman, A. M. Ferraria and A. M. Botelho do Rego, Characterization of wet-etched GaAs(100) surfaces, *Surf. Interface Anal.*, 2005, **37**, 673–682.
43 H. E. Swanson, *Standard X-ray diffraction powder patterns*, U.S. Dept. of Commerce, National Bureau of Standards, Washington, DC, 1953.
44 S. Sengupta, H. Loutati, K. Petel, E. Levin, N. G. Lemcoff and Y. Golan, The Effect of Short Chain Thiol Ligand Additives in Chemical Bath Deposition of Lead Sulphide Thin Films: the Unique Behaviour of 1,2-Ethanedithiol, *CrystEngComm*, 2016, **18**, 9122–9129.

